Lecture Notes in Civil Engineering

Serge Desjardins
Gérard J. Poitras
M. Shahria Alam
Xiomara Sanchez-Castillo *Editors*

Proceedings of the Canadian Society for Civil Engineering Annual Conference 2023, Volume 7

Materials Track

Springer

Lecture Notes in Civil Engineering

Volume 501

Lecture Notes in Civil Engineering (LNCE) publishes the latest developments in Civil Engineering—quickly, informally and in top quality. Though original research reported in proceedings and post-proceedings represents the core of LNCE, edited volumes of exceptionally high quality and interest may also be considered for publication. Volumes published in LNCE embrace all aspects and subfields of, as well as new challenges in, Civil Engineering. Topics in the series include:

- Construction and Structural Mechanics
- Building Materials
- Concrete, Steel and Timber Structures
- Geotechnical Engineering
- Earthquake Engineering
- Coastal Engineering
- Ocean and Offshore Engineering; Ships and Floating Structures
- Hydraulics, Hydrology and Water Resources Engineering
- Environmental Engineering and Sustainability
- Structural Health and Monitoring
- Surveying and Geographical Information Systems
- Indoor Environments
- Transportation and Traffic
- Risk Analysis
- Safety and Security

To submit a proposal or request further information, please contact the appropriate Springer Editor:

– Pierpaolo Riva at pierpaolo.riva@springer.com (Europe and Americas);
– Swati Meherishi at swati.meherishi@springer.com (Asia—except China, Australia, and New Zealand);
– Wayne Hu at wayne.hu@springer.com (China).

All books in the series now indexed by Scopus and EI Compendex database!

Serge Desjardins · Gérard J. Poitras ·
M. Shahria Alam · Xiomara Sanchez-Castillo
Editors

Proceedings of the Canadian Society for Civil Engineering Annual Conference 2023, Volume 7

Materials Track

Springer

Editors
Serge Desjardins
Department of Civil Engineering
Université de Moncton
Moncton, NB, Canada

Gérard J. Poitras
Department of Civil Engineering
Université de Moncton
Moncton, NB, Canada

M. Shahria Alam
School of Engineering
University of British Columbia, Okanagan Campus
Kelowna, BC, Canada

Xiomara Sanchez-Castillo
Faculty of Engineering
University of New Brunswick
Fredericton, Canada

ISSN 2366-2557 ISSN 2366-2565 (electronic)
Lecture Notes in Civil Engineering
ISBN 978-3-031-61510-8 ISBN 978-3-031-61511-5 (eBook)
https://doi.org/10.1007/978-3-031-61511-5

This Springer imprint is published by the registered company Springer Nature Switzerland AG
The registered company address is: Gewerbestrasse 11, 6330 Cham, Switzerland

Contents

Instrumentation of a Pavement Structure Containing Inductive Charging Equipment in the Canadian Context

Danial Arzjani, Diego Ramirez Cardona, Jean-Claude Carret, Jean-Pascal Bilodeau, and Sylvain Auger

Abstract Road transportation is a significant source of greenhouse gas emissions in Canada, and the use of electric vehicles (EVs) is an effective approach to reducing these emissions. With an inductive power transfer (IPT) system integrated into road structures, EVs can recharge their batteries while driving, allowing for longer distances without frequent stops for recharging. While the energy efficiency of induction charging has been demonstrated, few studies have examined the effects of adding inductive charging coils on the mechanical behavior and durability of pavement structures. Therefore, an experimental study will be conducted using a heavy vehicle simulator (HVS) on a laboratory test pit to analyze the behavior of two pavement structures containing induction charging loops under critical climatic circumstances for cold regions. Said structures were built in the accelerated testing facility at Laval University. The test pit was divided into three sections, two of them containing an inductive charging coil (Sections 1 and 2), placed between the base and surface course layers, and the third being a standard Quebec pavement structure without inductive equipment. The surface course thickness of Section 1 is 7 cm, while the other two sections have a surface course thickness of 5 cm. All sections have a consistent base course thickness of 12 cm and were built with the same asphalt mixtures. All three sections were instrumented with multiple sensors: strain gauges, load cells, and temperature and humidity probes. The sensors were placed at various positions

D. Arzjani (✉) · D. Ramirez Cardona · J.-C. Carret
École de Technologie Supérieure (ÉTS), Montréal, QC H3C 1K3, Canada
e-mail: Danial.arzjani.1@ens.etsmtl.ca

D. Ramirez Cardona
e-mail: Diego.Ramirez-Cardona@etsmtl.ca

J.-C. Carret
e-mail: Jean-Claude.Carret@etsmtl.ca

J.-P. Bilodeau · S. Auger
Laval University, Quebec City, QC G1V 0A6, Canada
e-mail: jean-pascal.bilodeau@gci.ulaval.ca

S. Auger
e-mail: sylvain.auger@gci.ulaval.ca

S. Desjardins et al. (eds.), *Proceedings of the Canadian Society for Civil Engineering Annual Conference 2023, Volume 7*, Lecture Notes in Civil Engineering 501,
https://doi.org/10.1007/978-3-031-61511-5_1

and depths during pavement construction to monitor the behavior of each component of the structures, from the surface course to the soil. The focus of this paper is to present the details of the construction and instrumentation of the test pit, which will be crucial for future accelerated loading tests and form the foundation for the development of design guidelines for inductive road structures in Nordic climates.

Keywords Pavement design · Electric road systems · Inductive dynamic charging · Pavements · Instrumentation

1 Introduction

The adoption of electric vehicles (EVs) and the implementation of electric roads (eRoads) are seen as ways to decarbonize the road transportation sector [1, 2], as the transportation sector is responsible for close to 25% of global greenhouse gas (GHG) emissions, 90% of which are generated by road transportation [3]. However, the limitations in battery technology, including limited driving ranges and high monetary and environmental costs due to the use of rare metals, hinder the widespread adoption of EVs [4]. To counter this, convenient and innovative charging options away from home must be developed, such as the concept of eRoads, which allow minimizing the size of the batteries, making them more practical, and efficient, thus reducing the EV's weight and energy consumption [5].

One of the main concepts in eRoads is contactless charging with inductive power transfer (IPT) technology, as shown in Fig. 1. Inductive eRoads present several advantages to contact-based solutions because the contactless technology does not affect traffic speed, does not alter the conditions of the pavement surface, and does not impose any limitations on the roadway geometry [6].

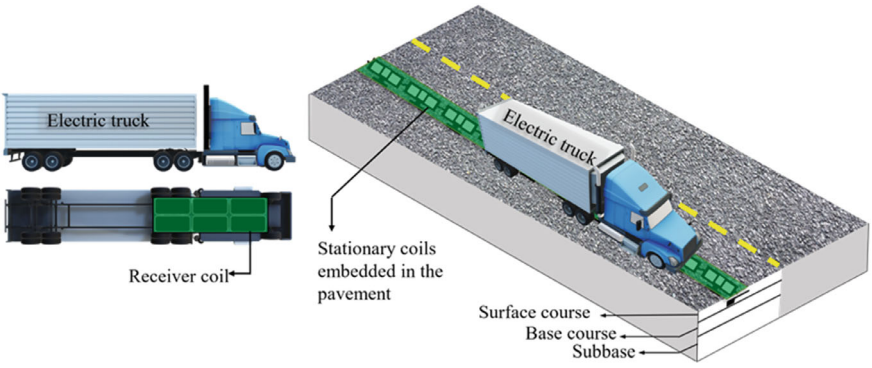

Fig. 1 Concept of inductive power transfer (IPT) technology in eRoads

In addition to the benefits mentioned, the inductive charging technology is also compatible with any battery technology and all types of electric vehicles, including heavy trucks and buses.

Despite the substantial growth of exploring IPT technology to power EVs over the last decades, the literature on the topic predominantly focuses on electric efficiency and transfer, with limited attention given to the pavement structural design and mechanical performance aspects. However, there is still a need for large-scale testing on road structures containing inductive charging coils, in order to study the impact of this technology on the mechanical performance and durability of pavements.

This paper presents the design, instrumentation, and construction process of a test pit on which response tests will be carried out to study the behavior of pavement structures incorporating IPT technology in Nordic climate conditions.

2 Structure Design

An eRoad structure, comprising a flexible pavement with two inductive charging coils, was constructed at the experimental pit of Laval University in Quebec, Canada.

The 4-m-long central section of the pit (total length is 6 m) was divided into three sections of equal lengths:

- "Section 1" (S1) was allotted for a 7-cm-thick surface layer and an embedded inductive coil.
- "Section 2" (S2) was allotted for a 5-cm-thick surface layer and an embedded inductive coil.
- "Control section" (CS) also has a 5-cm-thick surface layer and represents a conventional road pavement structure in Quebec.

The two 1-m-long sections at the pit's extremities are not considered to exclude the effect of wheel-entry vibrations.

All sections have a base course thickness of 12 cm. The surface layer thickness of 5 cm represents a conventional road pavement structure in Quebec. The thicker surface layer of 7 cm was chosen to be tested in order to study the influence of the asphalt mix thickness above the coils on the behavior of the eRoad pavement. Therefore, the total depth of asphalt is 17 cm for sections 2 and control, and 19 cm for section 1.

In order to have a flat and even surface on the whole test pit, a step of 2 cm was made in the subgrade between sections 1 and 2 (subgrade is 2 cm deeper in section 1) (see Fig. 2). Induction coils were cut to a length that allowed their installation in the limited space available in sections 1 and 2. The cut coil's length is 120 cm, and the length of each section is 133 cm. This geometric configuration will be considered in further analyses. The test pit schematics are depicted in Fig. 2.

In a real eRoad, the inductive charging coils are designed to be placed in the center of the lane, between the wheels of vehicles. However, in practice, the positioning of the vehicles and the resulting load distribution near the embedded coils may vary.

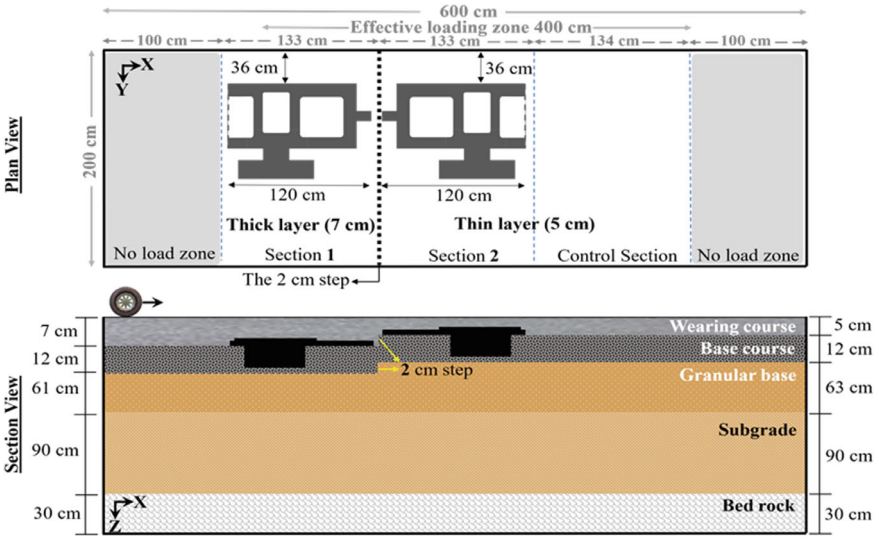

Fig. 2 Design of test pit for eRoad pavement at Laval University

For example, Fig. 3 describes two situations that can occur and where the load is either on the side or directly on top of the coils:

- "Situation 1," where drivers are driving in the center of the lane.
- "Situation 2," where drivers are not driving in the center of the lane or are changing lanes.

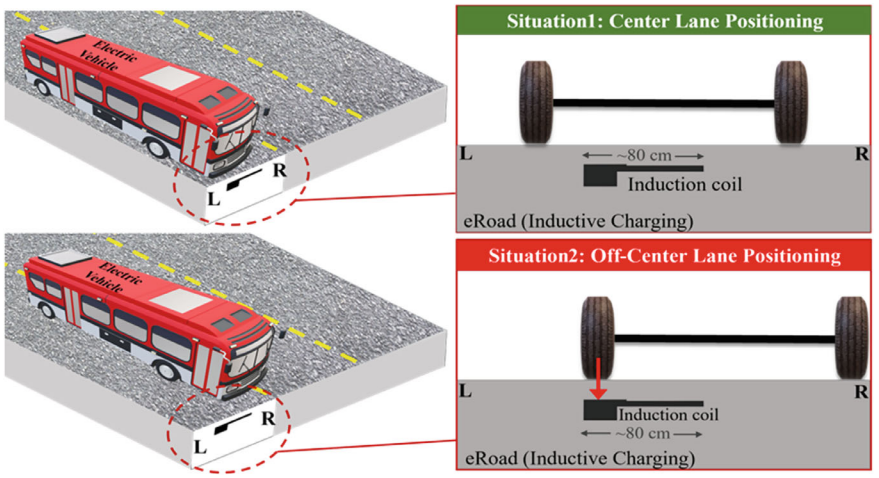

Fig. 3 Different driving situations that can occur on the road

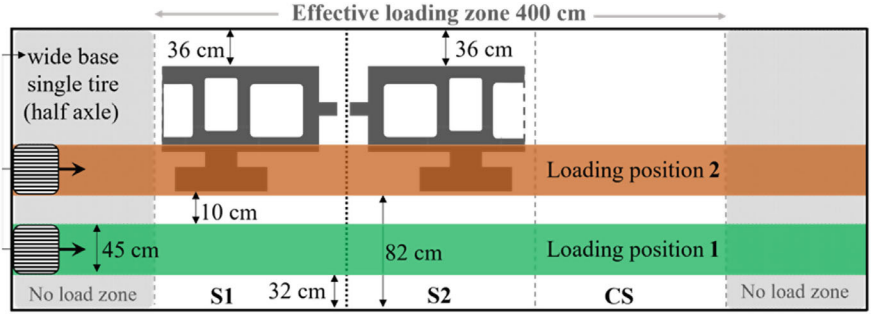

Fig. 4 Two extreme loading positions considered for the experiments in the test pit

Considering load situations 1 and 2 can occur on real eRoads, two extreme loading positions were proposed for the experiments in the test pit at Laval University (Fig. 4):

- "Loading position 1": the load is far away from the coils, representing Situation 1.
- "Loading position 2": the load is applied on top of the coil, representing Situation 2.

2.1 Inductive Coil

This research employed inductive charging coils made by Electreon Inc., a company that specializes in wireless charging technology for electric vehicles. The used inductive coils are illustrated in Fig. 5. However, in this project, given the limitations of the test pit size, the coils were cut to a length of 120 cm in order to fit them in their designated sections within the test pit.

2.2 Pit and Heavy Vehicle Simulator (HVS) Characteristics

The experimental pit, sized at 2 × 6 × 2 m, is divided into two parts with a 2 cm high step due to the difference in surface layer thickness (Fig. 2). The pit accommodates the ATLaS, a heavy vehicle simulator for full-scale accelerated pavement testing, allowing the simulation of field performance under accelerated traffic loads of 1 or 2 tires with loading range of 30–200 kN at speeds up to 13 km/h.

The simulator regulates air temperature, while the pit controls temperature at the bottom for experiments within a range of − 10 to 30 °C. To minimize heat transfer and speed up cooling, an isolating material was used. The pit is also equipped with a drainage and water injection system and has a layer of clean stone for even water distribution, regulated by an electronic level sensor.

Fig. 5 Electron inductive coil

2.3 Pit Materials

The granular base consists of MG-20 aggregates (Quebec Norm 2101). The asphalt base course and surface course were constructed using GB-20 and ESG-10 asphalt mixes (Quebec Norm 4202), respectively. Both mixes contained 20% reclaimed asphalt pavement (RAP) materials and had the same 58H-34 bitumen (Quebec Norm 4101). Both asphalt mixes correspond to commonly used materials in the construction of conventional high-traffic roads in Quebec. The maximum density of base course layer was 2518 kg/m^3, and surface course was 2518 kg/m^3.

2.4 Instrumentation

In order to characterize the strain levels in various areas of the pavement structure and analyze how the presence of the inductive coils affects these strains—particularly at the top and bottom of the coils and at the bottom of the base course—multiple strain gages were installed in the asphalt layers. Due to the thin layer of asphalt mix above the coils, thin strain gages (Dynatest PAST II) were used on top of the coils, while thicker strain gauges (TML KM-100HAS) were placed under the coils and at the bottom of the base course layer.

In addition, load cells were installed to measure pressure levels in the granular base, and temperature and moisture probes were placed at different depths in the structure to characterize the environmental conditions of the structure. Figure 6 shows

the global instrumentation of the structure in four plan views (a, b, c, and d), each one corresponding to one specific depth. "Plan d" illustrates the placement of Dynatest sensors on the coils, while "Plan c" shows the location of TML sensors, which were installed beneath the coils.

In addition, Table 1 summarizes the locations and types of sensors present in the pavement structure.

Load cells. Five load cells were used in this research to monitor the pressure level in the granular base. Load cells were placed in all three sections under the coils, at the same depths in the granular base corresponding to depths of 320 mm (S1) and 340 mm (S2 and CS) from the pavement surface. All the load cells are functional after the construction of the test pit.

Strain gauges. In this research, Dynatest and TML strain gauges were used to measure strains. Dynatest gauges were chosen for their thinness, allowing to instrument the top of the coils despite the thin layer of asphalt above them. TML gauges were used to measure strains in other parts of the structure, including under the coils. A total of 16 strain gauges were installed in the test pit, with 15 of them functioning properly after construction.

Moisture and Temperature probes. In this research, three volumetric moisture content sensors were installed beside load cells in each test section at the depths of 320 mm (S1) and 340 mm (S2 and CS) from the surface. Moreover, 48 thermistors were installed on 8 sticks that were inserted at different locations in the structure, allowing to draw a complete thermal profile of the pit.

In Fig. 7, all the sensors used in the test pit are displayed.

3 Construction and Installation Process

The construction of the test pit was carried out in three primary phases as illustrated in Fig. 8. The following paragraphs describe in detail the main activities carried out during the construction.

3.1 Subgrade and Granular Base Preparation and Instrumentation

Load cells were placed in designated locations in the granular base. A thermistor was located beside each cell. Moreover, the subgrade and granular base were instrumented with moisture sensors (ThetaProbe ML2). During the construction of the granular base, a rod equipped with six thermistors was inserted in the center of the pit, in order to characterize the vertical temperature profile in the granular layers.

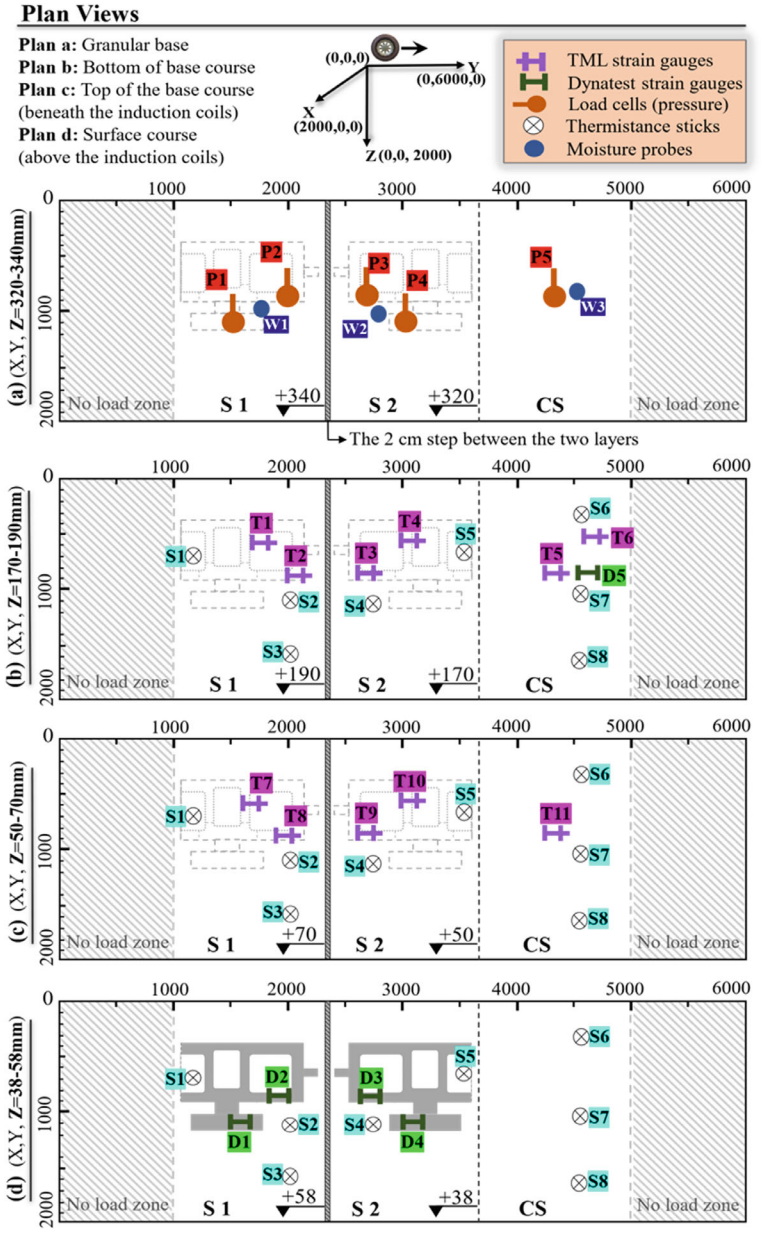

Fig. 6 Global instrumentation of the structure in four plan views: **a** at depth 320/340 mm; **b** at depth 170/190 mm; **c** at depth 50/70 mm; **d** at depth 38/58 mm

Table 1 Summary of the sensors' positions in the structure

Layer	Sensor type	Sensors positioning		
		S1	S2	CS
Surface course (Above the coil)	Strain gauge *(Dynatest PAST II)*	D1, D2	D3, D4	–
Base course (At the bottom)	Strain gauge *(TML KM-100HAS)*	T1, T2	T3, T4	T5, T6
Base course (at the top beneath the coils)	Strain gauge *(TML KM-100HAS)*	T7, T8	T9, T10	T11
	Strain gauge *(Dynatest PAST II)*	–	–	D5
Granular base	Load cell	P1, P2	P3, P4	P5
	Humidity probes *(ThetaProbe ML2)*	W1	W2	W3
All	Thermistance sticks*	S1, S2, S3	S4, S5	S6, S7, S8

*Each stick contains six thermistors (T0–T5); depths (mm) of thermistors for sticks S1–S4 are (10, 48, 56, 66, 114, 158); for stick S5 (10, 56, 63, 68, 117, 158); for sticks S6–S8 (10, 68, 76, 86, 135, 175)

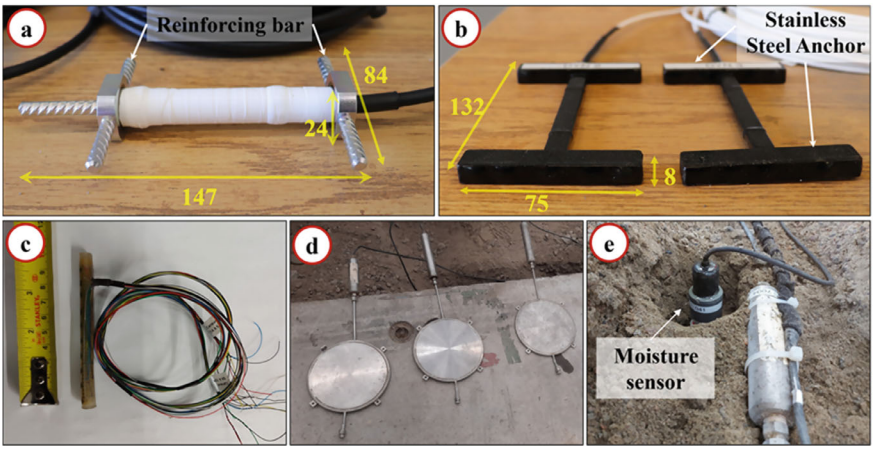

Fig. 7 Strain gauges. **a** TML gauges (24 mm thick); **b** Dynatest gauges (8 mm thick); **c** sticks containing thermistors; **d** load cells; **e** soil moisture sensor (ThetaProbe)

As previously stated, the granular base was constructed with a 2 cm step between sections 1 and 2. A wooden frame was used to maintain the shape of the step during the granular base compaction.

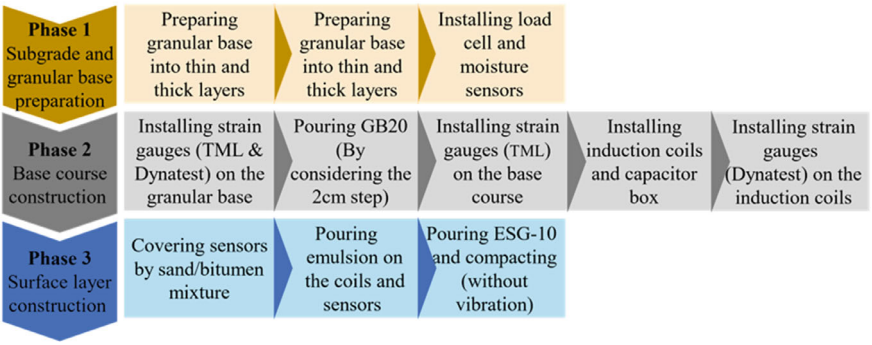

Fig. 8 Test pit construction process and main activities

3.2 Installation of the TML Gauges at the Top of the Granular Base

The process of installing strain gauges at the top of the granular base (bottom of the base course layer) involved several steps. First, the location of the sensors was marked on the granular base and on the sides of the pit for future reference. The sensors were then placed on a bed of sand/bitumen mix. To ensure proper contact, a metallic weight was placed on top of each sensor for more than 12 h. Finally, each sensor was coated with approximately 5–10 ml of fast-breaking bituminous emulsion (CSS-1).

In order to establish a correlation between the TML and Dynatest sensors, a Dynatest sensor was placed in the control zone, close to two TML sensors (see Fig. 6).

3.3 Construction of the Base Course Layer

The GB-20 layer was built after the installation of the strain gauges at top of the granular base. Each sensor was first covered with a small amount of sieved (5 mm sieve) hot asphalt mix. The uncompacted GB-20 mix was then poured manually due to the limited size of the test pit. The mix was then compacted carefully, assuring that the 2 cm level difference between sections 1 and 2 was maintained after compaction, while achieving the design's 12-cm-thick base course layer. A slope was created with the GB-20 mixture to ensure the transition between sections 1 and 2 over the step in the granular base.

Custom-made molds of the size of the TML strain gages were inserted into the surface of the asphalt mix before compaction, in order to create a void space to accommodate the TML gages at the top of the base course layer. To ensure the integrity of the sensors at the bottom of the base course layer, the GB-20 compaction

process was done with a compactor roller without the use of vibration. However, a vibrating plate was used to compact the borders of the pit.

3.4 Installation of the TML Gauges at the Top of the Base Course Layer

After compaction and cooling of the GB-20 layer, 5 mm deep trenches were carved at its surface in order to accommodate the TML gauges cables. After this, the TML-shaped molds were removed, and both sensors and cables were placed into their respective places.

A pure epoxy anchoring adhesive (Sika AnchorFix®-3001) was then poured around sensors and cables to fix them into the asphalt. The two-component epoxy was mixed thoroughly in a recipient before applying it, in order to trigger its hardening and increase its viscosity to prevent it from deeply penetrating the porosity of the asphalt.

3.5 Installation of the Coils with Capacitor Box

The coils' capacitor units were each placed in a hole (rectangular parallelepiped) created within the base course layer, after its construction. Such holes' dimensions are slightly bigger than the capacitor units. This installation configuration is of practical interest for the industry as it reduces the volume of asphalt that needs to be removed for the installation of the IPT equipment.

To achieve this, the contours of the holes were first sawed, followed by the remotion of the material using a combination of a core drill and a mechanical hammer. A heated asphalt mix was then poured and compacted at the bottom of the holes to ensure the correct level for the capacitor units.

The next step was to secure the capacitor units in place. A layer of epoxy resin was poured at the bottom of the holes and the capacitor units were placed inside. More epoxy resin was added to the sides to ensure a tight fit. The entire installation process is illustrated in Fig. 9.

Bituminous emulsion was then applied on top of the base course layer to cover all areas in contact with the coils. Finally, the coils were placed on top of the bituminous emulsion layer, and pressure was applied overnight to secure it in place.

Fig. 9 Capacitor unit installation process; **a** sawing, **b** coring; **c** compacting; **d** cleaning; **e** poring some asphalt and compacting; **f** fixing capacitor box with resin/epoxy

3.6 Installation of the Dynatest on Top of the Coils

Dynatest gauges on top of the induction coils were placed on a bed of hot bitumen (PG 58-28) at their designated locations. Sensors were secured by placing weights on top of them overnight. The gauges cables were glued to the coils with hot bitumen points.

To lead the cables out of the pit, small trenches were carved in the base course layer and a small slope was created on the rubber of the coils to guide the cables from the top to the trench in the asphalt. Figure 10 depicts installed strain sensors in various locations and layers.

Fig. 10 Installation of the strain sensors; **a** on the granular base layer (control section); **b** the TML sensors on top of the base course layer (beneath the coil); **c** the Dynatest strain gauges (on the coil)

Fig. 11 Construction operations; **a**, **b** granular base construction; **c** base course (GB-20) construction; **d** coils installation; **e** asphalt thickness measurements; **f** density measures with nucleodensimeter; **g** wearing course construction (ESG-10); **h** final result of the construction

3.7 Construction of the Surface Layer

The final step was the construction of the surface course. Base course, coils, and sensors were first coated with a conventional tack coat emulsion (Emulplus RC-CRS-1H). Then, the Dynatest gauges were covered with a 2–3-cm-thick layer of ESG-10 hot asphalt mix. A manual compaction plate was used to pre-compact the asphalt on top of the gauges. The rest of the ESG-10 mix was also poured manually, carefully filling the spaces inside the coils.

The asphalt was then compacted with a roller compactor without vibration. A vibrating plate was used to compact the borders of the pit. The top of the surface layer is at the same level as the top of the pit. Furthermore, following the construction of each asphalt layer, the density of the layers was measured using a nucleodensimeter in various sections. Figure 11 depicts all phases of the construction process.

4 Conclusions

A large-scale test pit was built in order to assess the mechanical behavior of pavement structures equipped with IPT charging equipment. Pavement structures with different wearing course thicknesses were built. Data collected from this large-scale test will serve for the calibration of a reliable numerical model of an eRoad pavement, which is the next step of the project. Such model will enable the proposal of

design recommendations for inductive roads, particularly adapted for cold regions. The details of the construction of the test pit are presented in this paper.

After construction, no evident defects were observed on the pit, in spite of the thinness of the surface course layers of the studied pavement structures, which correspond to conventional Quebec roads. The installation of IPT equipment in such structures is a novelty, as the surface course thickness of other test sections around the world is around 10 cm. Moreover, employing thin strain gauges for the instrumentation of very thin (> 5 cm) asphalt mix layers was successful.

The limited space available in the pit required the modification of the inductive coils, which needs to be considered during the future analysis of the data collected from the large-scale test. However, instrumentation presented enables the observation of local strain development that should be sufficient for the calibration of a complete numerical model of the inductive road structure.

The results from this global study aim at allowing the development of larger experimentation sites of inductive roads in Canada.

Acknowledgements The authors would like to express their gratitude to all individuals who have contributed to this project. Our sincere thanks go to our industrial partners, VINCI Construction Canada Inc. (previously Eurovia Canada Inc.) and Electreon Inc., and to PRIMA Québec for their support in providing the necessary resources to carry out this research.

References

1. Franzò S, Nasca A (2021) The environmental impact of electric vehicles: a novel life cycle-based evaluation framework and its applications to multi-country scenarios. J Clean Prod 315:128005. https://doi.org/10.1016/j.jclepro.2021.128005
2. Hawkins TR, Singh B, Majeau-Bettez G, Strømman AH (2013) Comparative environmental life cycle assessment of conventional and electric vehicles. J Ind Ecol 17(1):53–64. https://doi.org/10.1111/j.1530-9290.2012.00532.x
3. International Energy Agency (IEA) (2022) Greenhouse gas emissions from energy highlights. [Online]. Available: https://www.iea.org/data-and-statistics/data-product/greenhouse-gas-emissions-from-energy-highlights
4. Chen F, Taylor N, Kringos N (2015) Electrification of roads: opportunities and challenges. Appl Energy 150:109–119. https://doi.org/10.1016/j.apenergy.2015.03.067
5. Kalwar KA, Aamir M, Mekhilef S (2015) Inductively coupled power transfer (ICPT) for electric vehicle charging—a review. Renew Sustain Energy Rev 47:462–475. https://doi.org/10.1016/j.rser.2015.03.040
6. Soares L, Wang H (2022) A study on renewed perspectives of electrified road for wireless power transfer of electric vehicles. Renew Sustain Energy Rev 158:112110. https://doi.org/10.1016/j.rser.2022.112110

Creep Recovery Performance of Hydrated Lime (HL) and Limestone (LS) in RTFO Aged Asphalt Mastic

Shahrul Ibney Feroz, Ahmad Alfalah, Debzani Mitra, Kamal Hossain, Mitchell Lawlor, and Yosuf Mehta

Abstract In an asphalt structure, mastic is the primary element that deforms. Many studies have been conducted to develop a rheological parameter that can assess the deformation and creep characteristics of asphalt mastic with varying proportions of fillers. However, only a few studies show the influence of Hydrated Lime (HL), Limestone (LS), and their combined effect (HL + LS) on the creep recovery performance of asphalt mastic with the combination of modifiers and anti-stripping agents. This paper employs the multiple stress creep recovery (MSCR) test as per AASHTO T 350 to understand the creep recovery properties of asphalt mastic. This study modified a neat PG 58-28 binder with Styrene–Butadiene–Styrene (SBS) or Gilsonite and Zycotherm as a liquid anti-stripping agent. Different filler-binder (F/B) ratios of HL, LS, and different proportions of HL + LS combined with SBS and Gilsonite modified binder containing Zycotherm were utilized to fabricate the asphalt mastic. Then, the Rolling Thin-Film Oven (RTFO) protocol was applied to simulate asphalt production time aging. The performance of these mastics was compared using non-recoverable creep compliance, stress sensitivity analysis, and MSCR percent recovery analysis. AASHTO M 332 specifications have been used to classify all the mastics based on the

S. I. Feroz (✉)
Memorial University of Newfoundland, St John's, NL 1B 3X5, Canada
e-mail: siferoz@mun.ca

A. Alfalah · D. Mitra · Y. Mehta
Rowan University, Glassboro, NJ 08028, USA
e-mail: alfala19@students.rowan.edu

D. Mitra
e-mail: mitrad43@students.rowan.edu

Y. Mehta
e-mail: mehta@rowan.edu

K. Hossain · M. Lawlor
Carleton University, Ottawa, ON K1S 5B6, Canada
e-mail: kamal.hossain@carleton.ca

M. Lawlor
e-mail: MITCHELLLAWLOR@cmail.carleton.ca

S. Desjardins et al. (eds.), *Proceedings of the Canadian Society for Civil Engineering Annual Conference 2023, Volume 7*, Lecture Notes in Civil Engineering 501,
https://doi.org/10.1007/978-3-031-61511-5_2

Jnr value at 3.2 kPa and stress sensitivity. In addition, polymer modification curves specified by the asphalt institute (AI) were employed to interpret the test results. According to the analysis of experimental data, the combined effect of 10% HL and 70% LS modified with SBS was observed to be predominant and satisfy all the creep recovery performance requirements.

Keywords Asphalt mastic · Multiple stress creep recovery · Hydrated Lime (HL) · Limestone (LS) · Combined effect

1 Introduction

The component of the asphalt mixture known as the mastic deforms when stress is applied [1]. Mastic testing and research on the optimum filler-binder combination are subjects that are gradually garnering attention in this area and have demonstrated more potential than traditional binder testing [2, 3]. Asphalt mastic's cohesion and adhesion characteristics influence pavement performance [4]. In order to create asphalt mastic, fillers, a key component of the asphalt mixture's dispersion system, are often mixed with binder at certain ratios [5]. Most of this aggregate passes a 0.075 mm sieve [6]. With the inclusion of fillers, the cohesion between components formed mastic, where fillers influence the asphalt mixture by increasing the stiffness and altering the moisture resistance, workability, and compaction characteristics of asphalt mixtures [3, 7].

A filler's function in an asphalt mixture may be divided into the following separate actions: (1) functioning as an inert filler material (Limestone, dolomite, basalt, etc.) to fill spaces between coarse aggregates, and (2) acting as an active filler material (Hydrated Lime, fly ash, diatomite) when it encounters binder at the interface [8]. This study uses active filler Hydrated Lime (HL), which enhances the elasticity of asphalt mastic, lowers aging, and boosts moisture damage resistance [9]. Conversely, inert filler Limestone (LS) improves rutting performance by stiffening the asphalt mix. Thus, combining active and inert fillers can improve the rutting and moisture damage resistance. When the quantity of filler used exceeds a certain limit, thermal cracking may develop. This is because the filler particles are cementing the binder too strongly. Few studies were reported to investigate the combined effects of inert and active filler on the rheology-like creep recovery performance of asphalt mastic. Moreover, polymer-modified mastics offer more significant MSCR % recovery, whereas unmodified mastics show less MSCR % recovery [3]. High-temperature MSCR % recovery of modified asphalt mastic is yet to be evaluated. Hence, the present study investigated the high-temperature creep recovery performance of modified asphalt mastic fabricated with active, inert, or a combination of active and inert filler. The effect of asphalt mastic on various filler-binder ratios was also assessed using the MSCR test to determine the adequate amount of filler.

The MSCR test uses shear stress, and the test consists of 1 s creep followed by 9 s recovery. There are 10 cycles of creep, and recovery is done at two different

levels of stress: 0.1 and 3.2 kPa. The non-recoverable creep compliance (J_{nr}) and percent recovery (R) values are computed from the test results at both stress levels, as stated in the applicable AASHTO and ASTM standards [10, 11]. Jnr is recommended to represent the binder contribution to an asphalt mix permanent deformation. Another parameter, J_{nr} diff. values used to analyze an asphalt binder's stress sensitivity. However, this parameter is used in the mastic scales in this study. The MSCR % Recovery at 3.2 kPa is used to construct the polymer method MSCR curve to interpret the elastomeric performance of the RTFO aged asphalt mastic and ensure whether the samples are modified with an acceptable range with elastomeric polymer [11].

1.1 Objectives

- Evaluate the creep recovery performance of HL, LS, and combination of HL and LS in RTFO aged asphalt mastic containing modifiers and liquid anti-stripping agent based on non-recoverable creep compliance, MSCR % recovery at 3.2 kPa, and stress sensitivity.
- Compare the performance of SBS and Gilsonite to determine whether Gilsonite can be a viable alternative to SBS at high temperature and
- Investigate the effect of filler-binder (F/B) ratio on the creep recovery performance of RTFO aged asphalt mastic.

2 Materials and Methodology

2.1 Materials

Asphalt Binder. The selection of binder is crucial in preventing common pavement distresses such as rutting. For this study, PG 58-28 binder was chosen as the control binder based on its ability to perform well in extremely hot and cold climates. PG 58-28 was collected from McAsphalt.

Modifiers and Anti-stripping Agent. Two different modifiers were used in this study SBS (4% by the weight of base binder) and Gilsonite (10% by the weight of base binder) as shown in Fig. 1. Gilsonite and SBS were obtained from American Gilsonite Company and Yellowline Asphalt Products Limited, respectively. Liquid anti-stripping agent Zycotherm SP2 was added with the modified asphalt. Zycotherm SP2 was supplied by Zydex Industries, and it will be termed as Zycotherm throughout this study. 0.1% Zycotherm with 4% SBS and 10% Gilsonite showed better rutting performance in the previous study [12, 13]. So, 4% SBS, 10% Gilsonite, and 0.1% Zycotherm have been chosen in this study.

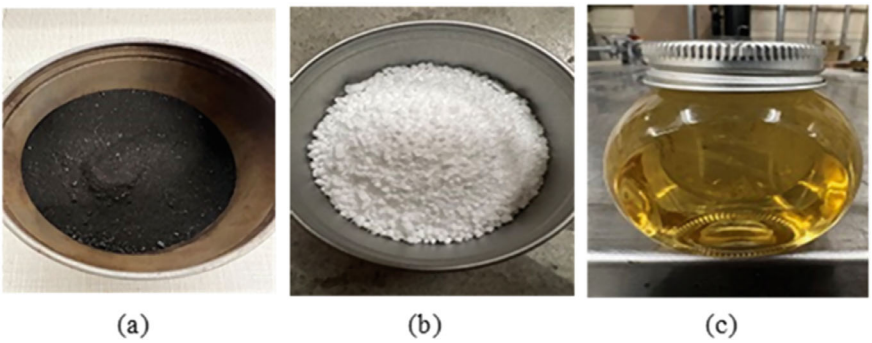

Fig. 1 Binder modifiers **a** Gilsonite, and **b** SBS and anti-stripping agent **c** Zycotherm

Fillers. Two different filler materials have been used in this study Hydrated Lime and Limestone. The hydrophilic coefficient of Hydrated Lime is 0.81, and for Limestone, it is 0.76. To evaluate the influence of the proportions of filler, three different F/B (0.3, 0.4, and 0.5 by the weight of the base binder) ratios of HL were used to prepare the asphalt mastic. Conversely, Limestone was obtained from Atlantic Minerals. The average size of the collected Limestone was 2–10 mm. To grind the materials, planetary ball mill equipment was used. After grinding the materials, the fine particles of LS were sieved with sieve No. 200. The LS powder passing sieve No. 200 was collected to use as a filler. The fillers are presented in Fig. 2. While preparing the mastic with LS, three different F/B ratios (0.7, 0.8, and 0.9 by mass) were used to evaluate the multiple stress creep recovery performance of asphalt mastic. The ideal filler content for modified mastic is between 0.8 and 1.2 [14]. Due to the considerable rise in mastic consistency, HL fillers must be introduced in small quantities. The F/B ratio was lowered to 0.3 after taking the absorption capacity test findings into account and an F/B range of 0.3–0.6 is advised to use [4]. Figure 3 displays scanning electron microscopy (SEM) imaging of the fillers. In the case of LS filler, most particles have a small grain size. In contrast, HL particles (Fig. 3a) are coarser, irregular, and porous. The mixture of HL and LS has well-graded particle size distribution with less porous. Asphalt binder with well-graded particle size distribution may improve the performance of asphalt mastics.

2.2 Methodology

Modification of Binder. Binders modified by SBS were prepared by preheating the control binder at 160 °C for 1 h. to make it fluid and SBS (4% by weight of base binder) were added and blended it for 45 min at 180 °C. Binders modified by Gilsonite were prepared by blending the preheated control binder with Gilsonite (10% by weight of base binder) for 30 min at 180 °C. Zycotherm, an anti-stripping agent, was added to both modified asphalts via a magnetic stirrer.

Fig. 2 **a** HL filler, **b** Limestone, and **c** LS filler

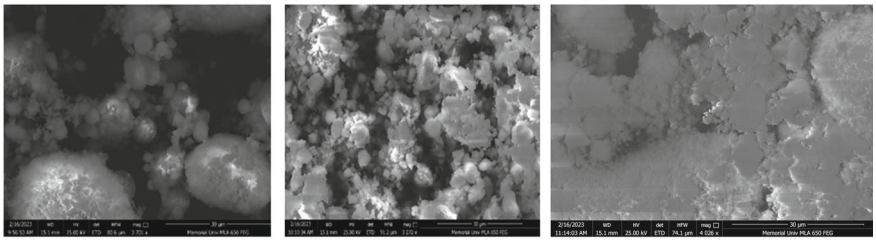

Fig. 3 SEM images of **a** HL filler and **b** LS filler **c** HL + LS filler

Sample Preparation of Asphalt Mastic. Prior to blending the fillers with the modified binder, each filler was cleaned and dried for 24 h at 105 °C in the oven. Modified asphalt and fillers were blended for at least 45 min at a temperature of 170 °C to create asphalt mastic using a hand stirrer. The filler was added gradually with the modified binder to avoid the filler sedimentation.

Aging, Testing, and Experimental Design. Finally, to simulate short-term laboratory aging of the base binders and modified binders, The Rolling Thin-Film Oven conditioning in accordance with AASHTO T 240 was employed. To prepare the RTFO aged samples, a continuous heat of 163 °C was applied to the binders for 85 min. Finally, the MSCR test protocol was employed using the DSR equipment. The testing temperature was 64 °C. There were 18 asphalt mastics containing different proportions of fillers. All the samples including the control binder tested twice to ensure the reliability of the data. The experimental plan of this study is illustrated in Fig. 4.

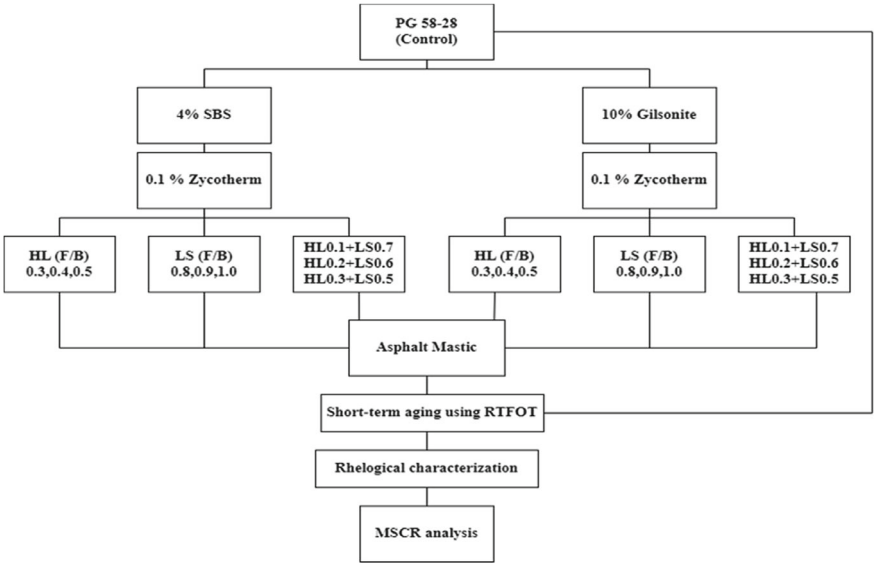

Fig. 4 Experimental plan

3 Results and Discussion

3.1 Non-recoverable Creep Compliance, J_{nr}

The J_{nr} is calculated to evaluate the deformation as per the AASTHO M 332. AASHTO M 332 specifications classify the binders as E (Extreme), V (Very heavy), H (Heavy), or S (Standard), as based on the J_{nr} value at 3.2 kPa. The J_{nr}, which is evaluated at 3.2 kPa, is used to assess the samples resistance to permanent deformation under repeated loading. A lower value of J_{nr} implies a lower rate of deformation, which implies higher rutting resistance [15].

Analysis of J_{nr} of SBS Modified Asphalt Mastic. The J_{nr} value for the RTFO aged PG 58-28 was 2.415 kPa^{-1} and in the binder level analysis, without the inclusion of any filler, J_{nr} value of SBS modified 0.1% Zycotherm was found 0.2 kPa^{-1} [12, 13]. Inclusion of filler (HL and LS) with SBS had considerably reduced the J_{nr} value (Fig. 5). SBS modified HL and LS filler mastics containing 0.1% Zycotherm had a decreasing pattern with the increase of the F/B ratios, while combination of HL and LS had an increasing pattern (Fig. 5). All the HL + LS mastics had a J_{nr} value less than the other mastics. The J_{nr} value was fluctuated between 0.012 and 0.016 kPa^{-1}. HL0.1 + LS0.7 had the lowest J_{nr} value with maximum rutting performance. Maximum J_{nr} value could be seen for LS when the F/B ratio is 0.8, which indicated the lower rutting performance in comparison with other mastics. Overall, SBS modified HL + LS and HL filler showed better rutting performance

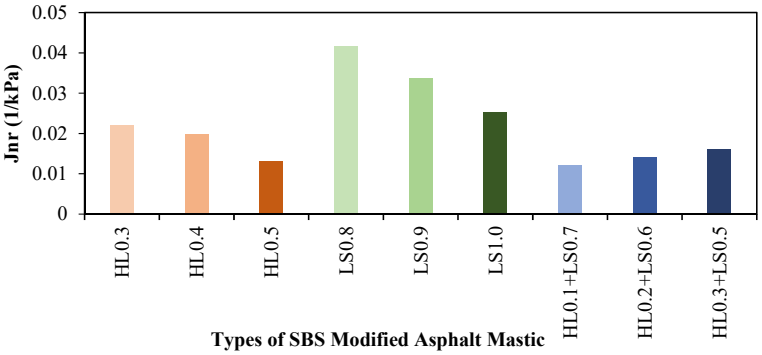

Fig. 5 Comparison of J_{nr} at 3.2 kPa^{-1} of HL, LS, and HL + LS SBS modified asphalt mastic

in comparison with LS mastics. Interaction between HL and LS and well-graded particle size distribution of the HL + LS mixture may be the possible reasons.

Analysis of J_{nr} of Gilsonite Modified Asphalt Mastic. Gilsonite modified 0.1% Zycotherm was found 0.25 kPa^{-1} in the previous investigation [12, 13]. According to Fig. 6, inclusion of filler (HL and LS), the J_{nr} values decreased and ranged from 0.02 to 0.11 kPa^{-1} for Gilsonite modified asphalt mastic which was very low and implied good rutting performance. However, the J_{nr} values for SBS modified mastics ranged from 0.012 to 0.04 kPa^{-1}. So, SBS modified mastics had 2.75 times lower J_{nr} values which implied better rutting resistance. Gilsonite modified HL, LS, and HL + LS filler mastics containing Zycotherm had same pattern as the SBS modified mastics although the J_{nr} values were more. HL0.1 + LS0.7 containing had the lowest value of J_{nr}. For both SBS and Gilsonite modified mastics, combination of HL + LS outperformed the HL or LS filler mastics.

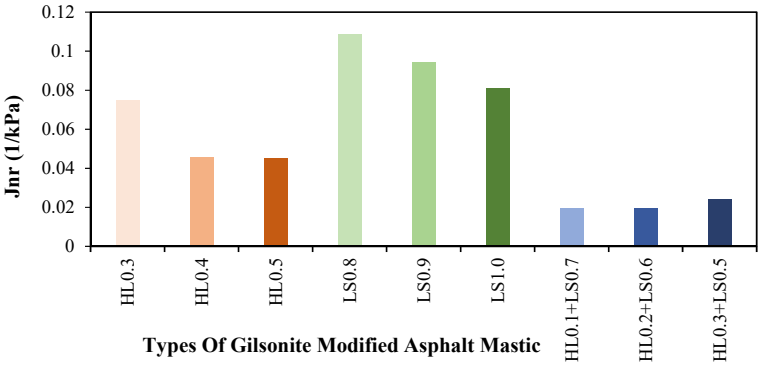

Fig. 6 Comparison of J_{nr} at 3.2 kPa^{-1}of HL, LS, and HL + LS Gilsonite modified asphalt mastic

3.2 Stress Sensitivity

Another critical parameter that can be measured from the MSCR test is stress sensitivity, which is used to measure the nonlinearity of asphalt mastic. MSCR test was conducted at 0.1 and 3.2 kPa. The difference in J_{nr} value at 0.1 and 3.2 kPa is used to measure the stress sensitivity of the asphalt mastics, as mentioned in Eq. 1 [16], However, there is a threshold value for this stress sensitivity, which is 75% based on AASHTO TP 70. Any asphalt mastic sample may fail if the stress sensitivity value crosses this threshold. Moreover, these samples are sensitive to higher stress and high temperatures in the field [17].

$$J_{nr,difference} = \frac{J_{nr,3.2\,kPa} - J_{nr,0.1\,kPa}}{J_{nr,0.1\,kPa}} \times 100\%, \tag{1}$$

where

$(J_{nr,difference})$ is the difference between the J_{nr} value at stress levels of 3.2 and 0.1 kPa;
$J_{nr,3.2\,kPa}$ is the J_{nr} value at stress levels of 3.2 kPa;
$J_{nr,0.1\,kPa}$ is the J_{nr} value at stress levels of 0.1 kPa.

Numerous studies have expressed concern regarding the applicability of this 75% threshold value due to the need for a relationship between J_{nr} difference and field performance [18–20]. Stempihar et al. solved the debate and proposed a new parameter [21]. J_{nr} slope in Eq. 2 is used to calculate the stress sensitivity. The new parameter works well for the modified binders and provides a comparable evaluation of stress sensitivity and low J_{nr} value at 3.2 kPa.

$$J_{nr,slope} = \frac{J_{nr,3.2\,kPa} - J_{nr,0.1\,kPa}}{3.1} \times 100\%, \tag{2}$$

where

$J_{nr,slope}$ is the proposed parameter for stress sensitivity;
$J_{nr,3.2\,kPa}$ is the J_{nr} value at stress levels of 3.2 kPa;
$J_{nr,0.1\,kPa}$ is the J_{nr} value at stress levels of 0.1 kPa.

Analysis of Stress Sensitivity of SBS Modified Asphalt Mastic. Figure 7 shows the comparison of stress sensitivity of SBS modified asphalt mastic with different F/B ratios of HL, LS, and HL + LS filler using the J_{nr} diff. parameter. All the mastics of HL and HL + LS passed the stress sensitivity criteria and less stress sensitive than the RTFO aged binder. Conversely, all the mastics of LS failed the stress sensitivity criteria.

The comparison of the modified method of stress sensitivity of SBS modified asphalt mastic with varying F/B ratios of HL, LS, and HL + LS is shown in Fig. 8 using the parameter J_{nr} slope. All the mastics passed the modified stress sensitivity criteria, whereas all the LS mastics contain failed to pass the previous stress sensitivity